Bioinspiration &
Biomimetics

NOTE • **OPEN ACCESS**

Skin deep: a novel biomimetic control strategy for rectilinear locomotion in snake robots

To cite this article: Henry C Astley 2026 *Bioinspir. Biomim.* **21** 044001

Bioinspiration & Biomimetics

NOTE

Skin deep: a novel biomimetic control strategy for rectilinear locomotion in snake robots

Henry C Astley*

Department of Biology, Biomimicry Research & Innovation Center, University of Akron, Akron, OH, United States of America
* Author to whom any correspondence should be addressed.

E-mail: hastley@uakron.edu

OPEN ACCESS

RECEIVED
2 September 2025

REVISED
7 May 2026

ACCEPTED FOR PUBLICATION
27 May 2026

PUBLISHED
10 June 2026

keywords: snake, rectilinear, robotics

Supplementary material for this article is available online

Abstract

Snakes are masters of movement through cluttered, confined, and complex habitats, leading to attempts to replicate this mastery in snake robots to improve our access to these challenging environments. While snakes use a variety of locomotor modes, rectilinear allows snakes to move through even the narrowest of spaces. However, while other modes are driven by axial bending, rectilinear relies on motion of the muscular skin, making it challenging to replicate in robots. Prior robotic rectilinear was achieved using secondary actuator systems (e.g. prismatic joints), anteriorly propagating waves, and/or standing waves, which require additional mechanical complexity, high vertical clearance, or dedicated parts for symmetry-breaking (e.g. electromagnets, deployable frictional pads), respectively. Here, I present a new algorithm which closely matches the robot to the motion of the snake's ventral skin (rather than the whole body) during rectilinear locomotion. Robot segments are assigned roles of either rigid ventral scales or flexible inter-scale skin. As in biological snakes, 'scale segments' are lifted clear of the substrate and moved forward via contraction and expansion of the adjacent 'skin motors'. This 'cutaneous rectilinear algorithm' allows rectilinear locomotion without the need for additional actuators or other specialized modifications, and achieves similar displacement per cycle and current consumption to propagating vertical wave methods at a lower vertical height, improving access to highly confined spaces.

1. Introduction

To effectively traverse the natural world, animals have evolved myriad adaptations which allow them exceptional capabilities across challenging environments and intense mechanical demands [1–4]. The desire to replicate these remarkable feats has led to bioinspired robots which can swim, run, jump, climb and fly [5–9]. Such bioinspired robots often have surprising solutions of mechanical challenges, and can outperform traditional robots, particularly in challenging natural environments such as sand, unstructured terrain, and complex flows [7, 10–15].

A common mechanical challenge is the need to move effectively through highly restricted and structurally complex environments, such as narrow pipes or densely cluttered structures, and for this application, snakes are an ideal model taxa [16–18]. The elongate body and highly diverse locomotor repertoire of snakes allows them to move rapidly and efficiently through environments which are difficult or impossible for other animals of equivalent mass. Indeed, their most recognizable form of locomotion, slithering, uses the environmental structures which are obstacles to limbed animals as propulsive 'push points' [19, 20], allowing them to increase their speed as obstacle density increases (up to a limit) [21] while limbed species must slow down [11, 22–25]. Unlike limbed species, which shift locomotor mode primarily based on speed (e.g. walk to trot to gallop) [26, 27], snakes shift locomotor mode based on substrate mechanics and geometry [20, 28–30], with over 20 described modes for environments ranging from loose desert sand to large tree branches to narrow tunnels [30].

Of crucial relevance to snake robots, rectilinear locomotion (figure 1) is often used to move through spaces only slightly larger than the snake's body [31–33]. Rectilinear locomotion is most easily elicited in heavy bodied vipers, pythons, and boas, but is present

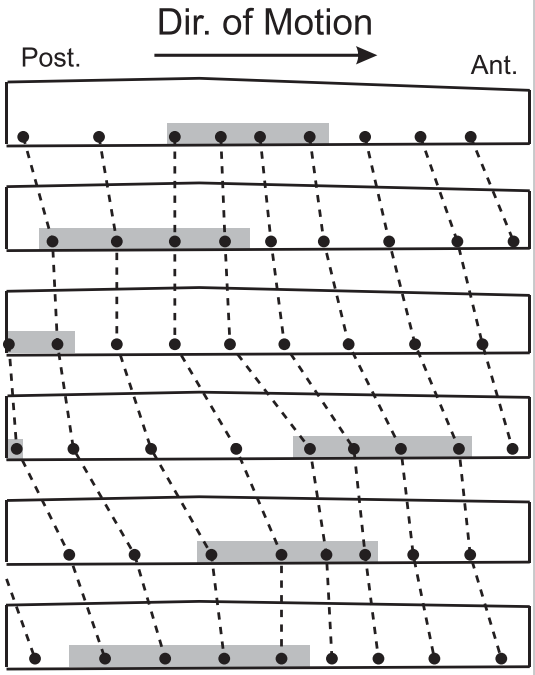

Figure 1. Diagram of rectilinear locomotion in snakes, showing a lateral view of a body segment. Points on the body are black dots, with dashed lines connecting the points over time (vertically downwards) to show motion. Regions of scales and skin are lifted and moved anteriorly, then lowered and placed into static contact with the ground (gray); posterior muscular force on the scales results in forward motion of the body. Image from [18], modified via creative commons.

in nearly all snakes as well as Amphisbaenian lizards (limbless except for genus *Bipes*) [34]. Unlike other modes of locomotion which are powered by bending of the vertebral column, rectilinear locomotion is powered by motions of the skin alone (figure 1), with no need for axial bending aside from turning [30–34]. During this mode, the enlarged ventral scales are pulled upwards and forwards relative to the ribs (which are held static or largely so) and the ground, stretching the skin posterior to the scale and contracting the skin anterior to it (figure 1) [30–35]; this mode seems to function whether the moving scale is fully lifted clear of the substrate or simply subject to lower pressure allowing easier sliding [32, 33]. The large ventral scale then makes firm static contact with the ground again, anchoring via friction as the skeleton and body are pulled forward over the snake, resulting in contraction of the posterior skin and stretching of the anterior skin (figure 1) [30–34]. These motions are repeated slightly out of phase in a posteriorly-propagating wave, resulting in multiple propagating regions of movement and stasis of the ventral skin along the body (figure 1) [30–34]. For a detailed examination of the kinematics, anatomy, and muscle activity, see [33].

For replication of rectilinear locomotion in bioinspired robots, the two crucial mechanical events are (1) the fore-aft motions of the ventral scales and (2) the ability to control contact forces (figure 1) [31, 33]. While in biological snakes, the expansion and contraction of the skin is largely driven by extrinsic muscles connecting to the ribs (the costocutaneous superior and inferior) [31, 33], the underlying physical principle is that the contact points are cyclically and forcefully displaced to produce net motion relative to the overall body. Robotic mechanisms to achieve this displacement are varied but generally fall into two categories—axial actuators and vertical bending [36–39]. Axial actuators include any actuation mechanism which increases and decreases the distance between adjacent robot segments, such as prismatic or lead-screw mechanisms with electric motors, pneumatics, electroactive polymers, etc [36–38, 40–43]; many such mechanisms could also be considered analogous to earthworms [44, 45]. Vertical bending can take the form of either standing waves which oscillate in amplitude (as in an inchworm caterpillar) [36, 46–51], or anteriorly-propagating waves[36, 39, 52–54], both using revolute joints across successive segments, as seen in many snake robots performing other locomotor modes [16, 55, 56]. While standing wave methods use amplitude changes of the standing wave to cyclically change the distance between the first and last segment, anteriorly-propagating waves use the discrepancy between path length of the body and distance between ground contact points to achieve forward displacement [36]. This last method is capable of quite high speeds [39, 53, 54, 57], but requires substantial vertical height changes to do so. Regardless of the mechanism used to displace contact points, effective forward motion requires some method of controlling contact point traction force, otherwise the robot will simply move in place with no net forward motion [36]. These can be in the form of directly actuated mechanisms such as grippers [40], electromagnets [46, 47, 51], shifting mass [48], or friction control via deployable frictional pads [37], ratcheting wheels [50], directional asymmetry in friction (passively or actively) [42, 43, 49], or simple lifting and lowering to make and break contact (as in the anteriorly-propagating waves) [36, 41].

As part of the extraordinary success of snakes in moving through cluttered, confined, and complex environments derives from their diversity of locomotor modes, an effective snake robot will ideally be able to implement multiple modes simultaneously [17, 18]. While a robot consisting of alternating vertical and horizontal motors can easily be programmed to produce sidewinding [58–60], lateral undulation [16, 61], and tunnel concertina locomotion [62, 63], rectilinear locomotion remains a challenge without secondary mechanisms as described above. The addition of axial actuators increases mechanical complexity and weight, as does the addition of actively controlled mechanisms to regulate contact, and asymmetric friction is often contingent upon the substrate properties. While an anteriorly propagating wave does

not require additional mechanical complexity, it does require greater changes in vertical height than axial actuator methods, which is counter to the role of rectilinear locomotion (and snake robots more broadly) in navigation of highly enclosed spaces.

I propose a new control algorithm, termed the 'Cutaneous Rectilinear Algorithm', based on close replication of the scale and skin motions observed in live snakes during rectilinear locomotion. This new algorithm allows any snake robot with vertical bending capability to achieve rectilinear locomotion, without the need for additional mechanisms or modifications. I hypothesize that the Cutaneous Rectilinear Algorithm will show comparable displacement per cycle to the vertical undulation algorithm, and while maintaining low vertical height and current consumption.

2. Methods

2.1. Cutaneous rectilinear algorithm

The cutaneous rectilinear algorithm's fundamental premise is to assign fixed identities to individual regions of the robot as either ventral scales (henceforth 'Scales') or inter-scale skin (henceforth 'Skin') (figures 2(A)–(E), Sup. Vids. 1 & 2). Scales consist of a single segment, while Skin regions consist of two or more segments in series and all motors connected to them (including those connected to the adjacent Scales) (figures 2(A)–(E), Sup. Vids. 1 & 2). In this paper, I tested versions of this algorithm with two and three segments in the Skin region, henceforth termed 'triangular' and 'rectangular', respectively, based on the shape when maximally contracted (figures 2 (A) and (G), Sup. Vids. 1 & 2). The first and last segments are Scale segments, with at least one additional Scale segment in between (two or three in this paper's implementation) (figures 2(A)–(E), Sup. Vids. 1 & 2). At the start of the cycle, all Scales are flat against the ground, and all Skin regions are maximally contracted except for the first, which is extended, with the segments straight and flat against the ground (figure 2(A), Sup. Vids. 1 & 2).

The procedure to move a Scale segment consists of three stages: Lifting, Scale Movement, and Lowering.

2.1.1. Lifting

First, the moving Scale is lifted above the ground by tilting the adjacent Skin regions (figure 2(B), Sup. Vids. 1 & 2). For the anterior Skin region, the anterior motor is dorsiflexed while the posterior motor is ventroflexed, while this is reversed in the posterior Skin region (figure 2(B), Sup. Vids. 1 & 2). Because the anterior Skin region is longer than the posterior one, imposing the same motor angle for lift in both resulting in poor contact and slipping. To mitigate this, the angle of lifting was adjusted via the law of sines, which showed that the ratio between the sines of the lifting angles for the anterior and posterior Skin regions was proportional to the ratio between the lengths of the anterior and posterior Skin regions. Since a peak of 5° of lifting was sufficient for ground clearance of the moving Scale, the small angle approximation allowed simplifying the ratio of sines to the ratio of angles (figure 2(B)). The initial lifting angle was 5° for the posterior Skin segment, with the anterior Skin segment angle calculated as above; this was recalculated through the subsequent commands during the

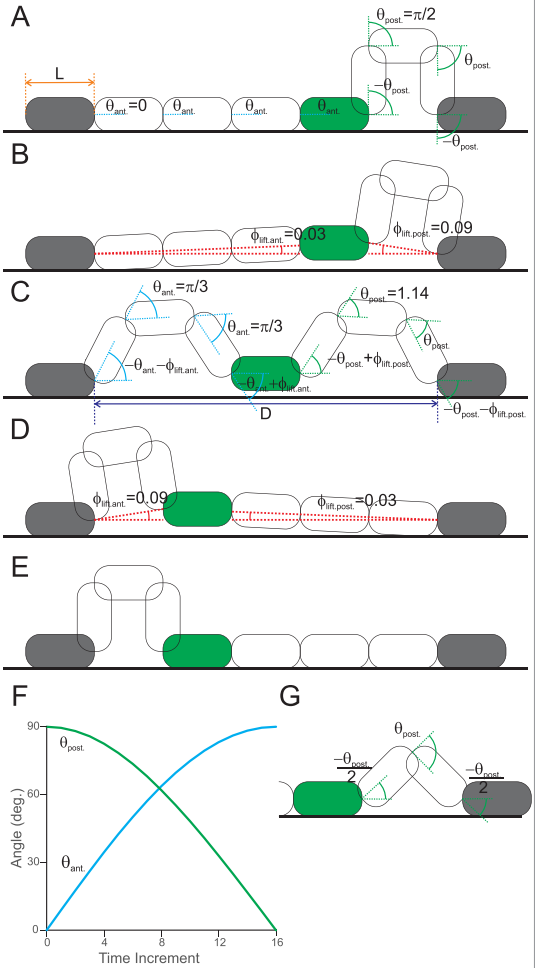

Figure 2. Control of the Cutaneous Rectilinear Algorithm in an example snake robot, moving toward the left. Static 'Scale' segments are gray, the moving 'Scale' segment is green, and 'Skin' segments are white. Segment length (L) is shown in A, while the length of the moving region (D) is shown in (C). (A) Initial position, using 'rectangular' variation (3 motors in 'Skin' segments). (B) The moving scale is lifted clear of the ground. (C) Synchronous contraction of the anterior 'Skin' region and extension of the posterior 'Skin' region translate the lifted 'Scale' forward, while it remains lifted. (D) Conclusion of motion. (E) The lifting offsets are returned to zero. The cycle can now repeat for the most posterior segment. (F) Angle change over 16 time increments for skin motors to ensure smooth motion. (G) Alternate angles for 'triangular' variation using 2 'Skin' motors.

second stage, with the anterior Skin segment being lifted at 5° at the end (figure 2(D)).

2.1.2. Scale movement

Second, the anterior Skin region is contracted while the posterior Skin region is lengthened (figure 2(B)–(D) Sup. Vids. 1 & 2). In order to prevent slipping at the adjacent static Scale segments, these changes had to be matched such that the total distance between static Scale segments (D) is constant. For a version with 3 segments and 4 motors in the Skin region ('rectangular'), the middle two motors will always be at equal angles while the outer two will be at that same angle in the opposite direction (aside from a pair of slight offsets to preserve lifting), thus each Skin region can be represented as a single angle, represented as q_{Ant} and q_{Post} (figure 2(B)). As we can neglect the small effect of lifting via the small angle approximation, the total distance between static Scale segments (D) for a robot with segment length L can be expressed as

$$D = 2L\cos\theta_{\text{Ant}} + 3L + 2L\cos\theta_{\text{Post}}.$$

For an initial position with $q_{\text{Ant}} = 0$ and $q_{\text{Post}} = \text{p}/2$, $D = 5\,\text{l}$ and thus the relationship between q_{Ant} and q_{Post} must be

$$1 = \cos\theta_{\text{Ant}} + \cos\theta_{\text{Post}}.$$

When using a 2 segment, 3 motor Skin region ('triangular') (figure 2(G)), we designate the middle motor of each Skin region as the defining angle of the region, with the anterior and posterior motors being half of this value, thus

$$D = 2L\cos\frac{\theta_{\text{Ant}}}{2} + L + 2L\cos\frac{\theta_{\text{Post}}}{2}.$$

For an initial position with $q_{\text{Ant}} = 0$ and $q_{\text{Post}} = \text{p}/2$, $D = 3\,\text{l} + \text{L}\sqrt{2} \approx 4.414\,\text{l}$ and thus the relationship between q_{Ant} and q_{Post} must be

$$1 + \frac{\sqrt{2}}{2} = \cos\frac{\theta_{Ant}}{2} + \cos\frac{\theta_{Post}}{2}.$$

To actuate the robot, q_{Ant} was defined, with q_{Post} computed according to the equations above. Initially q_{Ant} was computed via

$$\left[0, \frac{\pi}{2}\right] = \{i \in \mathbb{Z} | 0 \leqslant i \leqslant 16\}$$

$$\theta_{\text{Ant}} = i * \frac{\pi}{32}.$$

However, when q_{Ant} was changed linearly across its range, the arccosine necessary to compute q_{Post} resulted in changes in q_{Post} below the resolution of the motors at the start of the motion and excessively rapid movement of q_{Post} at the end of the motion, leading to slip and other abnormal motor behaviors. More specifically, at the start of motion, a change in q_{Ant} from 0 to p/32 would only produce a change of ∼p/300 in q_{Post}, corresponding to only two increments in the motor command position, while the final change in q_{Ant} from 15p/32 to p/2 would produce a change of ∼p/6 in q_{Post}, corresponding to a 170-fold increase in motor speed. Thus, to produce smoother motion and lower slip, q_{Ant} was computed$\theta_{\text{Ant}} = \frac{\pi}{2}\sin\left(\frac{i*\pi}{32}\right)$.

This resulted in calculated values of q_{Post} similar to (but not identical to) a cosine (figure 2(F)), which were more amenable to motor control. At the end of the motion, the anterior Skin region was maximally contracted, while the posterior Skin region was maximally extended (figure 2(D), Sup. Vids. 1 & 2).

2.1.3. Lowering

Finally, the lifting behavior was reversed, removing the offsets indicated previously and resulting in the moving Scale being laid flat against the ground, along with the posterior Skin region (figures 2(D)–(E), Sup. Vids. 1 & 2).

2.1.4. Subsequent scale movements

This behavior was then replicated for the next posterior Scale segment, with the now-extended Skin region becoming anterior and a new, contracted Skin region becoming posterior (Sup. Vids. 1 & 2). This was repeated for all scales, including the last one, which resulted in lifting both the first and last Scale segments as the most posterior Skin region contracts and the most anterior Skin region extends, restoring the initial position (Sup. Vids. 1 & 2).

2.2. Implementation & testing

To test the cutaneous rectilinear algorithm's efficacy and compare it to alternatives, I used a snake robot consisting of 12 Dynamixel XL330-M288-T motors (ROBOTIS, Inc., South Korea) connected via custom 3D printed brackets, with an inert 3D printed segment serving as the anterior-most segment. This robot was placed such that all motors axes were horizontal and produced vertical bending. The robot was controlled using an OpenRB-150 controller (ROBOTIS, Inc., South Korea) running with Dynamixel2Arduino library 0.7.0 (ROBOTIS, Inc., South Korea) and powered via a 6 V 2 A DC power source. Code is included in supplementary material.

We compared five rectilinear control algorithms which can be implemented without additional actuators or friction/contact manipulation. These included the 'rectanguar' and 'triangular' variations of the cutaneous rectilinear algorithm and three versions of the vertical undulation algorithm (Sup. Vids. 3–5); the maximum motor angle allowed by the robot joints was slightly more than 90°, thus the maximum angle was set to 90° for both cutaneous rectilinear algorithms (figures 2 (A) and (G), with vertical wave maximum amplitudes of 90°, 60°, and 30°. Each of the vertical undulation versions had two

complete waves on the body to always ensure at least two ground contact points, and differed only in maximum motor bending (30°, 60°, and 90°) (Sup. Vids. 3–5) [36, 39, 52–54]. While slightly higher values of maximum bending (100°) were mechanically possible without self-intersection, these values caused the robot to topple to the side within a cycle, and were not tested.

The snake robot was placed on a smooth, level sheet of expanded PVC for trials. Each control algorithm was tested in five trials, with each trial consisting of five cycles of motion. To quantify performance, here defined as distance moved per cycle, I attached two round, IR-reflective markers to the most anterior segment, and quantified the motions of these markers using a system of eight Flex13 infrared motion tracking cameras at 120 fps, connected to and controlled via Optitrack Motive software (NaturalPoint, Inc., Corvallis, OR, USA). These cameras recorded the 3D position of the markers with sub-millimeter precision.

To assess energetics, I used the internal current sensing capabilities of the Dynamixel motors, which summed current consumption across all motors for each cycle and exported it via serial connection. We measured the current consumed when the robot was static, and total current when moving, as well as the difference between the moving current and the mean static current of a given algorithm (to reduce extraneous variability). By separating these components out, I can distinguish the cost of maintaining a given posture, particularly one in which segments are actively elevated above the ground, from the actual cost of forward movement; this distinction is inspired by measurements of the energetics of terrestrial animal locomotion, which distinguishes the cost of movement (Net Cost of Transport, J per kg per meter) from the cost of stance and basal metabolic rate [64]. Cost of Transport (in Joules per meter) was calculated as the total current multiplied by the voltage (5 V) and cycle duration, divided by distance per cycle.

Finally, height was assessed by measuring the maximum vertical displacement during locomotion from the motion capture data for anteriorly-propagating waves. Because the most anterior segment did not elevate during the new rectilinear algorithm, vertical height was calculated from motor and bracket geometry and confirmed via static measurement. To confirm the ability of the rectangular algorithm to negotiate a tunnel lower than the quantified width, an additional video was recorded demonstrating this behavior in a tunnel of 7.5 cm height, constructed of the same expanded PVC material as the floor of the original test arena (Sup. Vid. 6).

All variables were compared using a single factor ANOVA with control algorithm as a fixed factor, and pairwise differences for significant effects assessed using Tukey's HSD.

3. Results

The cutaneous rectilinear algorithm achieved successful locomotion, defined as positive displacement per cycle for five continuous cycles (figure 3(A), Sup. Vids. 1 & 2). The 'triangular' implementation achieved similar but slightly lower displacement to the 30° vertical wave, and the 'rectangular' implementation achieved similar but slightly lower displacement to the 60° vertical wave; the 90° vertical wave achieved the highest displacement per cycle (figure 3(A)). All differences were statistically significant ($F_{4,120} = 13\,298$, $p < 0.0001$), and all pairwise comparisons were different.

Current consumption was also different across algorithms, with all current variables showing main effects ($F_{4,120} = 339$, $p < 0.0001$); all pairwise comparisons were different except for static current consumption, in which differences are denoted by letter (figure 3(C)). Static current consumption was highest for high-amplitude vertical waves, lowest for the cutaneous rectilinear algorithm, and intermediate for the 30° vertical wave (figure 3(C)). Total current consumption and differential current consumption (total-static) were both significantly different across algorithms (Total current: $F_{4,120} = 5772$, $p < 0.0001$, Differential current: $F_{4,120} = 3163$, $p < 0.0001$); all pairwise comparisons were significantly different. Current consumption increased with vertical wave amplitude and was higher in the rectangular than triangular cutaneous rectilinear algorithm (figure 3(C)). In all cases, the triangular rectilinear algorithm was cheapest, with the rectangular rectilinear algorithm being similar but slightly more costly than the 30° vertical wave for total current consumption and the 60° vertical wave for differential current consumption (figure 3(C)). When expressed in terms of energy consumed per meter moved, all algorithms were significantly different ($F_{4,120} = 2889$, $p < 0.0001$). Increasing vertical wave amplitude reduced cost of transport, and the rectangular cutaneous rectilinear algorithm was substantially lower cost than the triangular version, as well as being lower than the 30° vertical wave (figure 3(D)).

Both versions of the cutaneous rectilinear algorithm were substantially lower in height than the 60° and 90° vertical waves (figure 3(B)). The triangular version was slightly taller than the 30° vertical wave, while the 90° vertical wave was far taller than other algorithm (figure 3(A)).

4. Discussion

This paper demonstrates the proposed novel bio-inspired algorithm for snake robot rectilinear locomotion is effective (Sup. Vids. 1 & 2), and capable of achieving comparable locomotor performance to

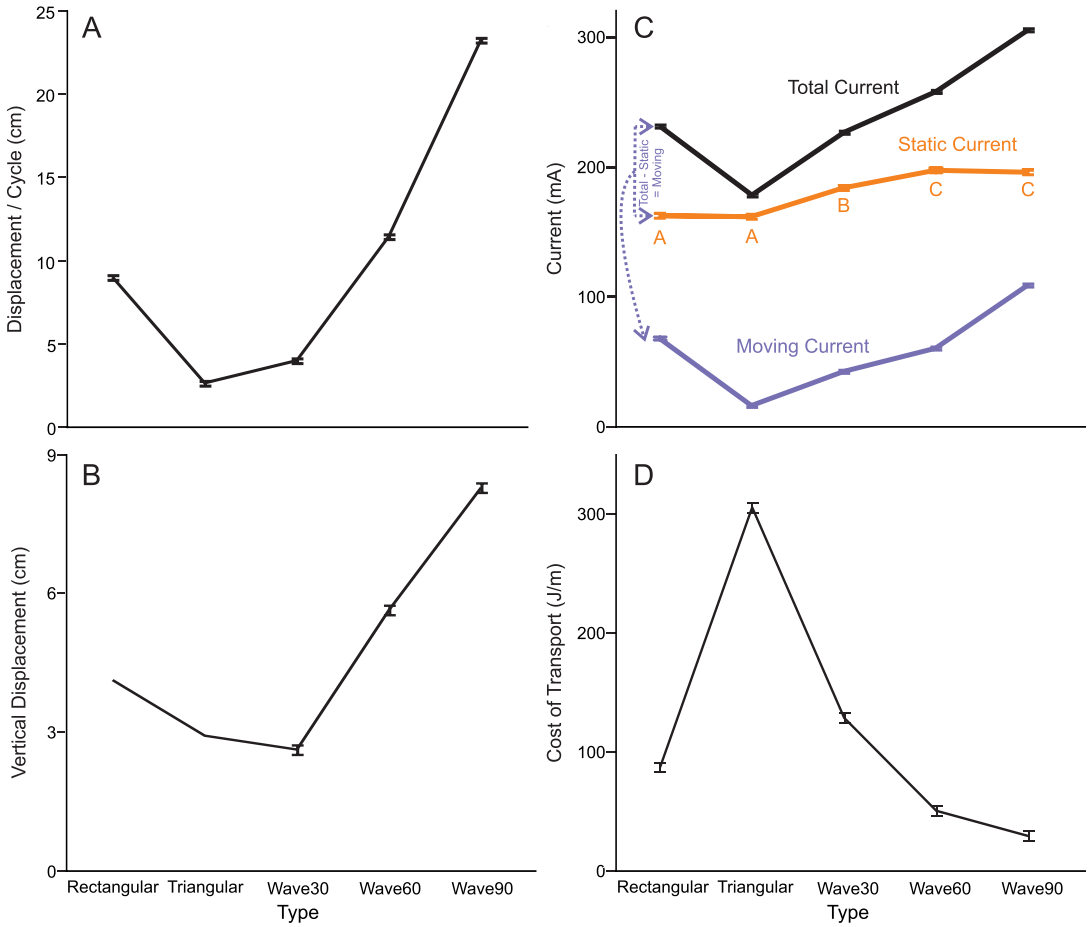

Figure 3. (A) Displacement per cycle, (B) Vertical displacement during a cycle, (C) Current consumption, showing total average current per cycle, current while maintaining a static posture, and moving current (= total—static), and (D) Cost of transport. All pairwise differences were significant except for static current, with letters showing the results of Tukey's honest significant differences. Error bars are omitted from cutaneous rectilinear algorithm vertical displacements, as these were measured from static height.

anteriorly propagating wave algorithms with similar or lower current cost for comparable performance and substantially lower vertical height (figure 3(B)). As a key purpose of snake-inspired robots is to access confined environments [16–18], this represents a significant advantage; the only situation in which rectilinear would be necessary but high-amplitude vertical wave algorithms would be superior is strongly laterally confined but vertically tall or unconfined environments. For extreme vertical height limitations, both the triangular version of the cutaneous rectilinear algorithm and the 30° vertical wave algorithm were similar in overall performance (figures 3 (A) and (B).

The relationship between displacement per cycle, vertical height, and motor parameters is a key difference between these algorithms (figure 3(A)). For vertical waves, vertical height and displacement per cycle are causally linked (figure 3(A)), and the relationship is largely independent of the motor number or their range of motion (provided they are sufficient to realize the commanded waveform). As the wave becomes higher amplitude, displacement and vertical amplitude both increase until a limit caused by geometric intersection of the waves; this intersection occurs well below the limits of the range of motion of the motors. Motor geometry affects this mode only insofar as it leads to toppling risk, with a narrower base reducing stability; this was observed directly in the slight deviations from a straight path in the 90° vertical wave (Sup. Vid. 5) and the toppling failures which prevented tests at higher amplitudes. However, in a laterally confined space, this may be irrelevant. In contrast, the cutaneous rectilinear algorithm is strongly influenced by the number of motors and their ranges of motion, as evidenced by the difference in performance between the rectangular and triangular versions (figure 3(A)). The fundamental mechanism of displacement in the cutaneous rectilinear algorithm relies upon the difference in length between the expanded and contracted Skin region (figures 2(A)–(E)), hence why the rectangular version (Extended Skin region Length = 3 l, Contracted Skin region Length = 2 l) outperforms the triangular version (Extended = 2 l, Contracted = 2 l*cos(p/4) = 2*L*0.707). Increased

number of motors would improve performance by allowing more complex geometries of the 'skin' segments both when maximally shortened and during the geometric changes from shortened to elongated or vice versa, but with a tradeoffs of vertical height; if motors remained limited to a maximum angle of 90°, a Skin region comprised of 6 segments and 7 motors in the shape of an W could theoretically exceed the displacement of the 90° vertical wave, but at the cost of greater vertical height. In contrast, increasing the motor range of motion could increase displacement per cycle without tradeoffs between displacement and vertical height, particularly in combination with increased number of segments in each Skin region; with a 180° range of motion, a Skin region of N segments could achieve a displacement of N * segment length while never exceeding a height of the segment length. Additional motors may also allow multiple moving scales at once, as in biological snakes (figure 1) [31, 33, 35]. Finally, the dramatic reduction in cost of transport between rectangular and triangular version of the cutaneous rectilinear algorithm suggests that future improvements may be able to achieve still greater energy savings. As such, the difference between these algorithms goes beyond the performance differences of these particular implementations, but in the scope of possible future innovations: the simplicity of vertical wave rectilinear offers easy control and high performance but little opportunity for future improvement, while the range of design space for the Cutaneous Rectilinear Algorithm is far greater than the two versions implemented here, particularly with corresponding hardware improvements.

This paper compares only two of the many known implementations of rectilinear locomotion (or similar movements) in snake-inspired robots [36, 37, 39, 41, 46, 49]. As explained above, these other implementations often rely on fundamentally different mechanisms, making direct comparisons meaningless, and require additional mechanical complexity. 'Inchworm' style robots [36, 47–49, 65] deserve special mention, as the cutaneous rectilinear algorithm could simply be thought of as two or more of such robots joined together and carefully coordinated. However, these standing-wave mechanisms require a method to break symmetry in order to achieve forward motion. While most such robots do so via dedicated secondary mechanisms or surfaces with anisotropic friction, the lifting and lowering of the middle 'Scale' segments to regulate contact (figures 2(A)–(E)) serves to break symmetry in the cutaneous rectilinear algorithm, allowing it to be implemented on any snake robot comprised of a series of servomotors capable of vertical motion, without further additions (figures 2(A)–(E), Sup. Vids. 1 & 2). Furthermore, by controlling contacts to maintain static posture at all ground contact points, this method should be less sensitive to terrain friction, and the algorithm could be easily modified to accommodate vertical unevenness in the terrain by simply increasing lifting height and biasing the anterior and posterior lifting angles. A snake robot comprised only of vertical and lateral bending motors (e.g. alternating servomotors) could be programmed to perform sidewinding [58–60], slithering (either planar or with both lateral and vertical combinations) [16, 61, 66], concertina [62, 63], and rectilinear locomotion, the four key 'categories' of snake locomotion (problematic as such categorization is, see [30]). This locomotor versatility is key to the success of snakes and will move bio-inspired snake robots incrementally closer to replicating their remarkable locomotor capabilities.

Acknowledgments

This work was supported by NSF BIO IOS Award #2045581 to HCA.

Data availability statement

The data that support the findings of this study is openly available at the following URL/DOI: https://doi.org/10.6084/m9.figshare.30024010 [67].

Author contribution

Henry C Astley 0000-0003-0136-1433
Conceptualization (equal), Data curation (equal), Formal analysis (equal), Funding acquisition (equal), Investigation (equal), Methodology (equal), Project administration (equal), Resources (equal), Software (equal), Supervision (equal), Validation (equal), Visualization (equal), Writing – original draft (equal), Writing – review & editing (equal)

References

[1] Hildebrand M 1985 *Functional Vertebrate Morphology* (Belknap Press of Harvard University Press)
[2] Nussbaum M C 1985 *Aristotle's de Motu Animalium: Text with Translation, Commentary, and Interpretive Essays* (Princeton University Press) (https://doi.org/10.2307/2025643)
[3] Biewener A A 2003 *Animal Locomotion* (Oxford University Press)
[4] Vogel S 2003 *Comparative Biomechanics: Life's Physical World* (Princeton University Press)
[5] Ayers J and Witting J 2007 Biomimetic approaches to the control of underwater walking machines *Phil. Trans. R. Soc. A* **365** 273

[6] Lauder G V, Anderson E J, Tangorra J and Madden P G A 2007 Fish biorobotics: kinematics and hydrodynamics of self-propulsion *J. Exp. Biol.* **210** 2767–80
[7] Benyus J M 2009 *Biomimicry : Innovation Inspired by Nature* (HarperCollins e-books)
[8] Flammang B E 2022 Bioinspired design in research: evolution as beta-testing *Integr. Comp. Biol.* **62** 1164–73
[9] Ishida M, Berio F, Di Santo V, Shubin N H and Iida F 2024 Paleoinspired robotics as an experimental approach to the history of life *Sci. Robot.* **9** eadn1125
[10] Daley M A, Usherwood J R, Felix G and Biewener A A 2006 Running over rough terrain: guinea fowl maintain dynamic stability despite a large unexpected change in substrate height *J. Exp. Biol.* **209** 171–87
[11] Sponberg S and Full R J 2008 Neuromechanical response of musculo-skeletal structures in cockroaches during rapid running on rough terrain *J. Exp. Biol.* **211** 433
[12] Mazouchova N, Gravish N, Savu A and Goldman D I 2010 Utilization of granular solidification during terrestrial locomotion of hatchling sea turtles *Biol. Lett.* **6** 398–401
[13] Li C, Hsieh S T and Goldman D I 2012 Multi-functional foot use during running in the zebra-tailed lizard (*Callisaurus draconoides*) *J. Exp. Biol.* **215** 3293–308
[14] Sefati S, Neveln I D, Roth E, Mitchell T R T, Snyder J B, Maciver M A, Fortune E S and Cowan N J 2013 Mutually opposing forces during locomotion can eliminate the tradeoff between maneuverability and stability *Proc. Natl Acad. Sci.* **110** 18798–803
[15] Karakasiliotis K, Thandiackal R, Melo K, Horvat T, Mahabadi N K, Tsitkov S, Cabelguen J M and Ijspeert A J 2016 From cineradiography to biorobots: an approach for designing robots to emulate and study animal locomotion *J. R. Soc. Interface* **13** 20151089
[16] Hirose S 1993 *Biologically Inspired Robots : Snake-like Locomotors and Manipulators* (Oxford University Press)
[17] Astley H C 2022 Slithering across worlds—snake-inspired robots for extraterrestrial exploration *Biomimetics in Aerospace* ed M Eggermont, V Shyam and A Hepp
[18] Tingle J L, Garner K L and Astley H C 2024 Functional diversity of snake locomotor behaviors: a review of the biological literature for bioinspiration *Ann. New York Acad. Sci.* **1533** 16–37
[19] Gray J and Lissmann H W 1950 The kinetics of locomotion of the grass snake *J. Exp. Biol.* **26** 354–67
[20] Jayne B C 1986 Kinematics of terrestrial snake locomotion *Copeia* **1986** 915–27
[21] Kelley K C, Arnold S J and Gladstone J 1997 The effects of substrate and vertebral number on locomotion in the garter snake *Thamnophis elegans Funct. Ecol.* **11** 189–98
[22] Collins C E, Self J D, Anderson R A and McBrayer L D 2013 Rock-dwelling lizards exhibit less sensitivity of sprint speed to increases in substrate rugosity *Zoology* **116** 151–8
[23] Parker S E and McBrayer L D 2016 The effects of multiple obstacles on the locomotor behavior and performance of a terrestrial lizard *J. Exp. Biol.* **219** 1004–13
[24] Gast K, Kram R and Riemer R 2019 Preferred walking speed on rough terrain: is it all about energetics? *J. Exp. Biol.* **222** 185447
[25] Clifton G T, Holway D and Gravish N 2020 Uneven substrates constrain walking speed in ants through modulation of stride frequency more than stride length *R. Soc. Open Sci.* **7** 192068
[26] Hoyt D F and Taylor R C 1981 Gait and the energetics of locomotion in horses *Nature* **292** 239–40
[27] Hildebrand M 1985 Walking and running *Functional Vertebrate Morphology* ed M Hildebrand, D M Bramble, K F Liem and D B Wake (Belknap Press of Harvard University Press) pp 38–57
[28] Mosauer W 1932 On the locomotion of snakes *Science* **76** 583–5
[29] Gray J 1946 The mechanism of locomotion in snakes *J. Exp. Biol.* **23** 101–20
[30] Jayne B C 2020 What defines different modes of snake locomotion? *Integr. Comp. Biol.* **60** 156–70
[31] Lissmann H W 1950 Rectilinear locomotion in a snake (*Boa occidentalis*) *J. Exp. Biol.* **26** 368–79
[32] Marvi H, Bridges J and Hu D L 2013 Snakes mimic earthworms: propulsion using rectilinear travelling waves *J. R. Soc. Interface* **10**
[33] Newman S J and Jayne B C 2018 Crawling without wiggling: muscular mechanisms and kinematics of rectilinear locomotion in boa constrictors *J. Exp. Biol.* **221** 166199
[34] Gans C 1975 Tetrapod limblessness: evolution and functional corollaries *Am. Zool.* **15** 455–67
[35] Petersen J C, Jayne B C, Wilde A D, Capano J G and Roberts T J 2024 Effects of ingesting large prey on the kinematics of rectilinear locomotion in *Boa constrictor J. Exp. Biol.* **227** 247042
[36] Chirikjian G S and Burdick J W 1995 The kinematics of hyper-redundant robot locomotion *IEEE Trans. Robot. Autom.* **11** 781–93
[37] Hopkins J K and Gupta S K 2014 Design and modeling of a new drive system and exaggerated rectilinear-gait for a snake-inspired robot *J. Mech. Robot.* **6** 021001
[38] Tang W, Reyes F and Ma S 2015 Study on rectilinear locomotion based on a snake robot with passive anchor. *2015 IEEE/RSJ Int. Conf. on Intelligent Robots and Systems (IROS)* pp 950–5
[39] Zarrouk D, Mann M, Degani N, Yehuda T, Jarbi N and Hess A 2016 Single actuator wave-like robot (SAW): design, modeling, and experiments *Bioinspir. Biomim.* **11** 046004
[40] Chen I-M, Yeo S H and Gao Y 2001 Locomotive gait generation for inchworm-like robots using finite state approach *Robotica* **19** 535–42
[41] Primerano R, Pietrocola A and Janko M A snake-like robot incorporating translational and rotation degrees of freedom *2013 IEEE/RSJ Int. Conf. on Intelligent Robots and Systems* 2013 pp 3279–84
[42] Saab W, Racioppo P, Kumar A and Ben-tzvi P 2019 Design of a miniature modular inchworm robot with an anisotropic friction skin *Robotica* **37** 521–38
[43] Marvi H, Meyers G, Russell G and Hu D L 2011 Scalybot: a snake-inspired robot with active control of friction *ASME 2011 Dynamic Systems and Control Conf. and Bath/ASME Symp. on Fluid Power and Motion Control* 2 (ASME) pp 443–50
[44] Garrey W E and Moore A R 1915 Peristalsis and coordination in the earthworm *Am. J. Physiol.* **39** 139–48
[45] Quillin K J 1999 Kinematic scaling of locomotion by hydrostatic animals: ontogeny of peristaltic crawling by the earthworm Lumbricus terrestris *J. Exp. Biol.* **202** 661–74
[46] Kotay K D and Rus D L 1996 Navigating 3D steel web structures with an inchworm robot *Proc. IEEE/RSJ Int. Conf. on Intelligent Robots and Systems IROS'96* vol 1 pp 368–75
[47] Kotay K and Rus D 2000 The inchworm robot: a multifunctional system *Auton. Robots* **8** 53–69
[48] Rincon D M and Sotelo J 2003 Ver-vite: dynamic and experimental analysis for inchwormlike biomimetic robots *IEEE Robot. Autom. Mag.* **10** 53–57
[49] Serrano M M, Chang A H, Zhang G and Vela P A 2015 Incorporating frictional anisotropy in the design of a robotic snake through the exploitation of scales *2015 IEEE Int. Conf. on Robotics and Automation (ICRA)* pp 3729–34
[50] Shi Z, Pan J, Tian J, Huang H, Jiang Y and Zeng S 2019 An inchworm-inspired crawling robot *J Bionic Eng* **16** 582–92
[51] Khan M B, Chuthong T, Danh Do C, Thor M, Billeschou P, Larsen J C and Manoonpong P 2020 iCrawl: an inchworm-inspired crawling robot *IEEE Access* **8** 200655–68
[52] Akbarzadeh A and Kalani H 2012 Design and modeling of a snake robot based on worm-like locomotion *Adv. Robot.* **26** 537–60
[53] Chang A H, Serrano M M and Vela P A 2016 Shape-centric modeling of traveling wave rectilinear locomotion for snake-like robots. *2016 IEEE 55th Conf. on Decision and Control (CDC)* pp 7535–41

[54] Virgala I, Kelemen M, Prada E, Sukop M, Kot T, Bobovský Z, Varga M and Ferenčík P 2021 A snake robot for locomotion in a pipe using trapezium-like travelling wave *Mech. Mach. Theory* **158** 104221
[55] Wright C *et al* Design of a modular snake robot *Proc. of the 2007 IEEE/RSJ Int. Conf. on Intelligent Robots and Systems* 2007 pp 2609–14
[56] Wright C *et al* Design and architecture of the unified modular snake robot. *IEEE Int. Conf. on Robotics and Automation* 2012
[57] Marín Arciniegas J J, Vivas Albán O A, Marín Arciniegas J J and Vivas Albán O A 2023 Design and construction of a snake-like robot implementing rectilinear and sidewinding gait motions *TecnoLógicas* **26**
[58] Burdick J W, Radford J and Chirikjian G S 1993 A "sidewinding" locomotion gait for hyper-redundant robots. *Proc. IEEE Int. Conf. on Robotics and Automation, IEEE Comput. Soc* (Press) pp 101–6
[59] Marvi H, Gong C, Gravish N, Astley H, Travers M, Hatton R L, Mendelson J R, Choset H, Hu D L and Goldman D I 2014 Sidewinding with minimal slip: snake and robot ascent of sandy slopes *Science* **346** 224–9
[60] Astley H C *et al* 2015 Modulation of orthogonal body waves enables high maneuverability in sidewinding locomotion *Proc. Natl Acad. Sci. USA* **112** 6200–5
[61] Kano T, Yoshizawa R and Ishiguro A 2016 TEGOTAE-based control scheme for snake-like robots that enables scaffold-based locomotion *Lecture Notes in Computer Science (Including Subseries Lecture Notes in Artificial Intelligence and Lecture Notes in Bioinformatics)* vol 9793 (Springer) pp 454–8
[62] Yoshizawa R, Kano T and Ishiguro A 2016 *Realization of Snakes' Concertina Locomotion by Using "Tegotae-based Control* (Springer) pp 548–51
[63] Astley H C Traversing tight tunnels—implementing an adaptive concertina gait in a biomimetic snake robot 2018 *Earth and Space 2018, 16th Biennial Int. Conf. on Engineering, Science, Construction, and Operations in Challenging Environments* (American Society of Civil Engineers) pp 158–68
[64] Bennett A F 1985 Energetics and locomotion *Functional Vertebrate Morphology* ed M Hildebrand, D M Bramble, K F Liem and D B Wake (The Belknap Press of Harvard University) pp 173–84
[65] Cao J, Liang W, Wang Y, Lee H P, Zhu J and Ren Q 2020 Control of a soft inchworm robot with environment adaptation *IEEE Trans. Ind. Electron.* **67** 3809–18
[66] Jurestovsky D J, Usher L U and Astley H C 2021 Generation of propulsive force via vertical undulations in snakes *J. Exp. Biol.* **224** jeb239020
[67] Astley Henry 2026 Raw Data for "Skin Deep: a novel biomimetic control strategy for rectilinear locomotion in snake robots" *Figshare* (available at: https://doi.org/10.6084/m9.figshare.30024010)